



## City Research Online

### City, University of London Institutional Repository

---

**Citation:** Villoslada, D., Santos, M. & Tomas-Rodriguez, M. (2022). TMD stroke limiting influence on barge-type floating wind turbines. *Ocean Engineering*, 248, 110781. doi: 10.1016/j.oceaneng.2022.110781

This is the accepted version of the paper.

This version of the publication may differ from the final published version.

---

**Permanent repository link:** <https://openaccess.city.ac.uk/id/eprint/27810/>

**Link to published version:** <https://doi.org/10.1016/j.oceaneng.2022.110781>

**Copyright:** City Research Online aims to make research outputs of City, University of London available to a wider audience. Copyright and Moral Rights remain with the author(s) and/or copyright holders. URLs from City Research Online may be freely distributed and linked to.

**Reuse:** Copies of full items can be used for personal research or study, educational, or not-for-profit purposes without prior permission or charge. Provided that the authors, title and full bibliographic details are credited, a hyperlink and/or URL is given for the original metadata page and the content is not changed in any way.

---

---

---

City Research Online:

<http://openaccess.city.ac.uk/>

[publications@city.ac.uk](mailto:publications@city.ac.uk)

---

# 1 TMD Stroke Limiting Influence on Barge-type Floating Wind Turbines

2  
3 D. Villoslada\*

4 University Complutense of Madrid, Computer Sciences Faculty, 28040-Madrid, Spain

5 [davillos@ucm.es](mailto:davillos@ucm.es)

6  
7 M. Santos

8 Institute of Knowledge Technology, University Complutense of Madrid, 28040-Madrid, Spain

9 [msantos@ucm.es](mailto:msantos@ucm.es)

10  
11 M. Tomás-Rodríguez

12 The City, University of London, London, UK.

13 [Maria.Tomas-Rodriguez.1@city.ac.uk](mailto:Maria.Tomas-Rodriguez.1@city.ac.uk)

14  
15 \* Corresponding author: Daniel Villoslada. Computer Sciences Faculty, C/ Profesor García  
16 Santesmases 9, UCM, 28040-Madrid, Spain. Email: [davillos@ucm.es](mailto:davillos@ucm.es)

## 17 18 19 **Abstract.**

20 In this paper, passive structural control techniques are applied to a barge-type Floating Offshore Wind  
21 Turbine (FOWT) to mitigate the impact of pendulum effect loads. The passive structural control device, a  
22 tuned mass damper (TMD) installed in the nacelle, is analyzed on a reduced dynamics FOWT model.  
23 Genetic algorithms are used for the optimization process, taking the tower fatigue as the fitness function,  
24 implemented as the standard deviation of the fore-aft tower top displacement. The optimization of the TMD  
25 shows that its resulting stroke is unfeasible in terms of space needed for installation. Therefore, the addition  
26 of stroke-limiting stops to the TMD should be considered. A new optimization, including stops, yields a  
27 clear improvement of the device performance while limiting the stroke to the nacelle dimensions. It is  
28 observed that the stops allow to mitigate the second collective platform pitch-tower bending mode in  
29 addition to the first one. Finally, a third case is presented, considering the whole stops configuration as  
30 additional variables in the optimization loop. This last case improved the TMD performance in terms of  
31 vibration suppression rate, proving the effectiveness of optimizing stops for mass and space constrained  
32 applications.

33

34 **Keywords:** Barge-type floating offshore wind turbine, passive structural control, optimization, genetic  
35 algorithms, TMD stroke, stops.

## 36 **1 Introduction**

37 Wind is a renewable source of energy that is efficiently helping to mitigate climate change negative  
38 impact. This clean energy reduces environmental pollution by replacing other more polluting resources,  
39 such as fossil energy (Mikati et al., 2013). But the field of onshore wind turbines (WT) seems to have  
40 reached a high degree of exploitation and technological maturity. To expand the harnessing of the wind to  
41 more promising areas, offshore wind turbines started to be developed a few decades ago (Costoya et al.,  
42 2020). Initially, coastal wind turbines were installed in shallow waters, where winds were stronger and  
43 more stable (Caglayan et al., 2019). Nevertheless, the deployment and maintenance of these turbines is  
44 implied high costs, whilst they do not really solve the problem of acoustic and visual impact, neither some  
45 negative effects on marine animals and birds, and they affect tourism and property values. These are some  
46 of the reasons that have triggered the installation of wind farms in deeper waters.

47 Conventional offshore wind turbines are installed on fixed foundations laying on the seabed, making  
48 them unsuitable for waters more than 50 m deep. As an alternative, floating wind turbines (FOWT) are  
49 offshore WTs mounted on a floating structure that allows the turbine to generate electricity in deep waters  
50 in comparison to the traditional bottom-fixed ones. In addition, the cost of installation is reduced as  
51 assembly is simplified, deployment is more flexible, inspections and maintenance are easier, and the  
52 environmental impact is reduced. FOWTs not only allow to diminish the acoustic and visual impact, but  
53 also reduce the seabed footprint and so the damage to the abundant coastal flora and fauna. An increasing  
54 industrial and commercial interest in these types of energy harvesting systems is observed nowadays.

55 Floating offshore wind turbines use new concepts of foundation, which are technically feasible for its  
56 deployment on waters from 60 to 900 meters depth. FOWTs are divided into three major types, depending  
57 on the restoring mechanism they rely on. The main stabilizing methods are buoyancy, ballasting, and

58 mooring. The derived floating foundation types are the barge, the spar buoy, and the tension leg platform  
59 (Wang et al., 2010).

60 The present study focuses on barge-type floating wind turbines, which stand out for their simple design,  
61 assembly, and maintenance benefits. The stability of this concept is achieved through its waterplane area  
62 moment and the mooring forces from the catenary lines.

63 Preliminary load analysis carried out by Jonkman and Buhl (2007) on a wind turbine installed on a  
64 barge-type floating platform. It was shown that waves and wind induced motions that increased the  
65 displacements and loads on the structure due to an inverted pendulum effect. Even more, the relative  
66 structural fatigue between the sea-based and land-based turbines increases from the blade tip to the tower  
67 base, reaching unacceptable figures.

68 A promising approach to reduce FOWT loads is the application of structural control, which have been  
69 successfully used for decades in civil engineering to protect structures from damage caused by dynamic  
70 loading such as earthquakes, wind, or traffic (Saaed et al., 2015). The application of these control devices  
71 to offshore wind turbines has been a topic of interest the last years (Yang et al., 2019a). Structural control  
72 can be considered as an additional Degree of Freedom (DOF) added to the structure, instead of an  
73 intervention of the existing turbine power control system. If sufficient, the main benefit of the structural  
74 control application would be not to require any design alteration from the baseline land-based wind turbine.

75 Among the three major types of structural control, which are passive, semi-active, and active, this work  
76 focuses on the passive approach. Within this type, energy dissipation devices are the ones of interest and,  
77 more specifically, the dynamic vibration absorbers (DVA). They typically consist of a mass resonant device  
78 attached to the structure by a spring and a viscous damper (Tomás-Rodríguez and Santos, 2019). This  
79 combination is usually referred to as a Tuned Mass Damper (TMD). The tuning of the TMD parameters is  
80 a crucial process, typically carried out by adapting the spring stiffness and the damper constant to bind the  
81 TMD resonance frequency to one of the system natural frequencies, which maximizes energy absorption  
82 (Yang et al., 2019a).

83 The effectiveness of a TMD device is directly proportional to its mass (Stewart and Lackner, 2013).  
84 However, the more massive the TMD is, the longer its stroke and thus, more room is required for its  
85 installation. In order to consider the space limitations of the nacelle, where these devices are usually  
86 installed, stops are introduced in the form of additional springs and dampers at both ends. This generates  
87 nonlinearities, giving rise to a more complex dynamics of the system. Moreover, in the case of limiting  
88 stops being present, the tuning of the stop devices may be considered as additional variables to be optimized.  
89 This results in a larger optimization problem that, to the best of the authors' knowledge, has not been  
90 addressed before in other studies.

91 In order to provide plausible and practical solutions, this work analyses the feasibility of passive  
92 structural control in barge-type FOWTs. Reducing the platform oscillations and structural vibrations  
93 improves the system's efficiency and decreases the structural fatigue. Therefore, a TMD is installed in the  
94 nacelle. Using a reduced dynamic FOWT model, the TMD is optimized to reduce the collective platform  
95 pitch-tower bending mode of the floating turbine. The design process adds stops that limit the TMD stroke  
96 to fit it into the nacelle. As the addition of stops to the TMD modifies the system's dynamics, various  
97 optimizations were carried out to analyze the dependency of the wind turbine efficiency with respect to the  
98 stops configuration and, besides, to study the energy absorption in the frequency and time domain.

99 Another interesting contribution of this work is the inclusion of the TMD stops in the mathematical  
100 model of the FOWT. Indeed, the novelty of this work lies in the fact that usually stops are not considered  
101 as part of the TMD passive control, and when they are included, the optimization of the stroke of the TMD  
102 is carried out independently from the wind turbine behaviour. In this paper, equations have been obtained  
103 to represent the action of these stops on the dynamics of the floating wind turbine.

104 Simulation experiments have been carried out on the 5-MW NREL (National Renewable Energy  
105 Laboratory) barge-type floating wind turbine, using FAST-SC (Fatigue, Aerodynamics, Structures, and  
106 Turbulence), the high-fidelity simulation software developed by Lackner and Rotea (2011b), that includes  
107 structural control functionalities. Interesting and novel conclusions have been obtained regarding the  
108 mitigation of the main frequency modes of the floating device.

109 This paper is organized as follows: Section 2 summarizes some related works. The reduced model of  
110 the floating wind turbine used is described in Section 3. The passive structural control device, including the  
111 stops, is also modelled in this section. Section 4 shows the optimization process for tuning the TMD  
112 parameters. In Section 5 the optimization of the TMD with stops under different configurations is presented.  
113 Results are discussed. The paper ends with the conclusions and suggestions for future works.

## 114 **2 Related works**

115 Although relatively recent, the field of FOWT has already gathered a substantial amount of research  
116 devoted to improving the efficiency of these type of systems (Lackner and Rotea, 2011b). The approaches  
117 taken in the current existing literature cover a wide range of areas of specialization, depending mainly on  
118 the objectives to be achieved (Pimenta et al., 2020). The general goal has been to provide a robust and  
119 maximized energy production (Olondriz et al., 2019; Rubio et al., 2019; Sierra-García and Santos, 2020a;  
120 Sierra and Santos, 2021). More specifically, the application of structural control to offshore wind turbines  
121 has been a topic of interest the last years (Sierra-García and Santos, 2020b; Park et al., 2019; Zuo et al.,  
122 2020). Passive control devices have started to be widely applied yielding good results in terms of load  
123 mitigation and vibration control.

124 In Lackner and Rotea (2011a), passive and active control were investigated for a floating barge-type  
125 wind turbine. Optimal parameters are determined using a parametric study of the tuned mass damper device.  
126 The performance was evaluated as a function of the active power consumption and the stroke of the  
127 actuator. The obtained results showed that active control is effective in reducing structural loads, but at the  
128 expense of active power and large strokes. Also (Lackner and Rotea, 2011b) applied two TMDs located in  
129 the nacelle of the turbine model, with one TMD in the fore-aft direction, and the other in the side-side  
130 direction. The stiffness, damping and external force of each TMD were controllable. An analysis was done  
131 to determine the optimal parameters of a passive single DOF, fore-aft, TMD system in both a barge-type  
132 and monopile support structure.

133 Most of these control devices are installed in the nacelle, although sometimes they are located in the  
134 tower of spar-buoy wind turbines (Dinh and Basu, 2015), and much less frequent, in the barge supporting  
135 platform (Galán-Lavado and Santos, 2021). In any case, the design of the TMD involves the optimization  
136 of its parameters, i.e., stiffness, damping, mass and location, to effectively reduce the vibrations of the wind  
137 turbine. To mention a few examples. Stewart and Lackner (2013) used FAST-SC to assess passive control  
138 solutions for both tension leg platforms and barge-type floating wind turbines. They used a TMD located  
139 in the nacelle. He et al. (2017) derived a linear model of barge type floating wind turbine with a fore–aft  
140 tuned mass damper in the nacelle. The dynamic responses of the wind turbine with/without tuned mass  
141 damper were simulated and the suppression effect of the tuned mass damper was investigated over a wide  
142 range of load cases. In Liao and Wu (2020), a novel concept of a passive FOWT structure is proposed to  
143 overcome the previous limitations of space and mass of tuned mass dampers. The conceptual design was  
144 examined on the basis of a finite element model with promising results. In Xie et al. (2019a) a coupled  
145 aero-hydro-servo-elastic model of a barge-type wind turbine was developed and simulated for different  
146 load cases. An optimized TMD was installed in the nacelle. The time-domain and frequency-domain  
147 analysis of simulation results indicated that the designed TMD could significantly inhibit the structural  
148 loads and stabilize the electrical output power. Some other studies have considered the stroke as a constraint  
149 in the TMD optimization (Yang and He, 2020; Chen et al., 2021). Nevertheless, this work does not use  
150 stops to limit the stroke as we propose in here.

151 At present, the methods to adjust TMD parameters are frequency tuning, genetic algorithms (GA), and  
152 surface plot (Yang et al., 2019b). The surface plot approach is usually discarded as it required a considerable  
153 computational cost. According to these authors, although the frequency tuning method is an effective  
154 approach to find the optimum TMD parameters, it has some limitations. Therefore, the use of GAs to  
155 optimize TMD design has grown in recent years. Indeed, Yang et al. (2019b) applied frequency formulas  
156 and GA to tune the TMD for the same wind turbine model and obtained a better suppression rate of  
157 vibrations with the evolutive technique.

158 As mentioned, the inclusion of the TMD stops is scarce in the turbine-related literature although some  
159 notable exceptions can be found. Hu and He (2017) investigated an active vibration control strategy for a  
160 barge-type floating wind turbine by setting a stroke-limited hybrid mass damper (HMD) in the turbine's  
161 nacelle. The stroke of the active damper and the active control power consumption were the constraints. Li  
162 et al. (2017) used a fore–aft tuned mass damper in the nacelle/tower subsystem to design passive control of  
163 a semi-submersible offshore wind turbine. The corresponding mass, stiffness and damping parameters of  
164 the TMD in this case were optimized using both exhaustion and genetic algorithm methods, to avoid local  
165 minimums. Nevertheless, these studies assumed the stops to be fixed parameters, hence they were not  
166 optimized. In Villoslada et al. (2020), the authors explored the addition of a passive inerter parallel-  
167 connected to a TMD in the nacelle. Stops were used to limit the stroke, in this case, only the actuation  
168 distance was optimized.

169 Similarly, the work by Park et al. (2019) focused on a magnetorheological damper and its significance  
170 on the structural control of a tension leg platform. A parametric study was carried out to determine the  
171 optimal parameters of a passive TMD tuned to the first tower natural frequency. The stops were not included  
172 in the design process. Xie et al. (2019b) used a single degree of freedom tuned mass damper (TMD) system  
173 installed in the platform. To achieve the ideal response mitigation effect, they analyzed the TMD  
174 configuration. The stops were not optimized and were fixed. Yang et al. (2019b) also included stops in a  
175 TMD model fitted in the platform of a barge-type wind turbine; in this case the stroke was not considered  
176 either perhaps due to the fact that space limitation in the platform is not a usual problem.

177 Cong included the nonlinearity due to space constraints of the wind turbine, which impacts on the  
178 vibration control (Cong, 2019). This work studies active tuned mass dampers with constrained stroke in the  
179 vibration control of the blades and lateral (side-side) tower vibration of an on-shore wind turbine.

180 Although the issue of the stroke limitation of TMDs installed in FOWTs is somehow addressed in the  
181 literature, for barge-type wind turbines these stops are fixed to a value that –in the best-case scenario- has  
182 been obtained from the parametric analysis of the passive control device. Thus, the main difference of the  
183 work here presented from those existing previously is that in our case, the optimization process, using

184 genetic algorithms, includes the stroke in the optimization loop and explores the benefits of including the  
 185 stops configuration as additional tuning variables.

### 186 **3 FOWT and TMD Model**

187 The baseline floating offshore wind turbine used in this study is the National Renewable Energy  
 188 Laboratory (NREL) 5-MW wind turbine (Jonkman et al., 2009). It is a horizontal-axis, three-bladed,  
 189 upwind, variable speed, pitch-controlled turbine with a 126 m rotor diameter and a 90-meter hub height.  
 190 The main parameters and geometrical properties are summarized in Table 1. This turbine has been adopted  
 191 as a reference model by many research projects supported by the U.S., the European Union UpWind  
 192 research program, and the International Energy Agency. It is a rather large rating turbine, whose size was  
 193 assumed to be the minimum to make a FOWT economically viable, because of the large proportion of costs  
 194 devoted to the support platform.

195 The 5-MW wind turbine is mounted on a barge design developed by the Department of Naval  
 196 Architecture and Marine Engineering at the Universities of Glasgow and Strathclyde under a contract with  
 197 ITI Energy (Vijfhuizen, 2006). To ensure simplicity in manufacturing, the barge has a squared shape and  
 198 is ballasted with sea water to achieve the designed draft. Eight catenary lines moor the platform preventing  
 199 it from drifting. The barge main characteristics are provided in Table 2.

200

201 Table 1. Gross properties of the NREL 5-MW Baseline Wind Turbine (Jonkman et al., 2009)

Rating	5 MW
Rotor Orientation, Configuration	Upwind, 3 Blades
Control	Variable Speed, Collective Pitch
Drivetrain	High Speed, Multiple-Stage Gearbox
Rotor, Hub Diameter	126 m, 3 m

Hub Height	90 m
Cut-In, Rated, Cut-Out Wind Speed	3 m/s, 11.4 m/s, 25 m/s
Cut-In, Rated Rotor Speed	6.9 rpm, 12.1 rpm
Rated Tip Speed	80 m/s
Overhang, Shaft Tilt, Precone	5 m, 5°, 2.5°
Rotor Mass	110,000 kg
Nacelle Mass	240,000 kg
Tower Mass	347,460 kg
Coordinate Location of Overall CM	(-0.2 m, 0.0 m, 64.0 m)

202

203

Table 2. Gross characteristics of the ITI Energy Barge (Vijfhuizen, 2006)

Size (W×L×H)	40 m × 40 m × 10 m
Moonpool (W×L×H)	10 m × 10 m × 10 m
Draft, Freeboard	4 m, 6 m
Water Displacement	6,000 m <sup>3</sup>
Mass, including Ballast	5,452,000 kg
Center of Mass (CM) below SWL	0.282 m
Roll Inertia about CM	726,900,000 kg·m <sup>2</sup>
Pitch Inertia about CM	726,900,000 kg·m <sup>2</sup>

Yaw Inertia about CM	1,453,900,000 kg·m <sup>2</sup>
Anchor (Water) Depth	150 m
Separation Between Opposing Anchors	773.8 m
Unstretched Line Length	473.3 m
Neutral Line Length Resting on Seabed	250 m
Line Diameter	0.0809 m
Line Mass Density	130.4 kg/m
Line Extensional Stiffness	589,000,000 N

204

205 In this paper, the structural control of the barge-type win turbine is implemented by using a tuned mass  
206 damper (TMD) system. These devices are very efficient for vibration reduction. They consist on a mass,  
207 stiffness elements (springs), and dampers. When a structure vibrates, the fitted TMD vibrates at the same  
208 structure's frequency but out of phase. The TMD inertial force reduces the vibrational energy transmitted  
209 to the system which dissipates in the form of heat. These systems are referred as "tuned" because the mass  
210 and springs are tuned, or adjusted, to the structural mode (i.e. the natural frequency) of the structure to be  
211 damped. Usually this is the first vibrational mode (first natural frequency), since it plays the most significant  
212 role in a system's response.

213 Thus, the three configuration parameters of the TMD that much be tuned are:

- 214 • Mass,  $m_T$  (kg): the larger the TMD mass is, the greater inertia will be and therefore, the greater  
215 amount of stored kinetic energy.  $m_T$  is usually limited to a ratio of the total mass of the structure.
- 216 • Spring stiffness coefficient,  $k_T$  (N/m): is defined as the proportionality of the resultant spring force  
217 in relation to its compression / extension.

218 • Damping coefficient,  $d_T$  (N·s/m): regulating the magnitude of the resultant force proportional to the  
219 relative speed between the ends of the damping element, i.e., between the mass and the structure.

220 In addition to the above-mentioned parameters, the TMD design process often considers other factors  
221 such as:

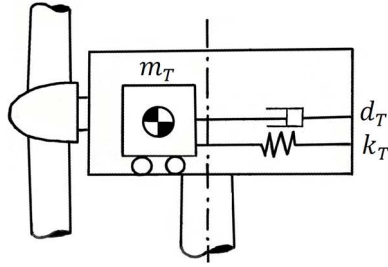
222 • TMD position. The TMD can be fitted in any part of the FOWT, i.e., in the nacelle, in the tower or  
223 in the platform. The exact location this device will impact the magnitude and frequency of the loads  
224 suffered by the TMD, as well as other design constraints.

225 • TMD orientation: usually referred to a wind-aligned reference system. The most common TMD  
226 orientation is fore-aft, which means downwind, or side-side if lateral vibrations are to be considered.

227 • Stroke limits. Stops can be installed to limit the stroke of the TMD mass. The logic of this action  
228 must be also considered.

229 There are some studies that analyse the dynamical behavior of FOWT depending on the TMD location  
230 and the type of floating wind turbine, the later limits the possible locations of the TMD (Dinh and Basu,  
231 2015; Yang et al., 2020). In the case of a barge-type FOWT, the TMD could also be fitted in the platform  
232 with the objective of absorbing energy. However, there are three main drawbacks for this approach. First,  
233 the platform pitch, although highly energetic in absolute terms, does not display large motions. This means  
234 that the installation of a short stroke TMD would require a large mass. Secondly, the orientation of a TMD  
235 in the nacelle is always aligned with the fore-aft direction because the nacelle's yaw control turns the rotor  
236 towards the upwind direction, whereas if the TMD is fitted in the platform it sustains a steady predetermined  
237 direction that not always would be aligned with the external disturbances (wind and waves). Third, it has  
238 been shown that the benefits of a TMD fitted on a barge-type FOWT platform are less significant than when  
239 this is fitted in the nacelle (Yang et al., 2019b; Galán-Lavado and Santos, 2021). Even in a spar wind  
240 turbine, the nacelle TMD optimally tuned is seen to be more effective than the spar TMD (Dinh and Basu,  
241 2015).

242 Several analyses of FOWT have shown that fore-aft oscillations have more influence on tower base  
 243 loads than side-side oscillations (Jonkman, 2007). In this work, the authors consider the TMD to be fitted  
 244 in the nacelle and towards the fore-aft direction. A schematic layout is shown in Figure 1.



245  
 246

Figure 1. TMD fore-aft oriented in the nacelle of the floating wind turbine

247 In order to use the 5-MW NREL FOWT as a benchmark, a simple and efficient model is to be included  
 248 in the optimization loop. A reduced model containing the two fundamental modes of the structure that  
 249 contribute the most to the tower base loads (Jonkman, 2007) is used in this work. These modes are the  
 250 platform pitch and the tower fore-aft displacement. The optimization process focuses on tuning the TMD  
 251 to the collective platform pitch-tower bending modes. No external disturbances (wind or waves) have been  
 252 considered. The dynamic model of the floating system is obtained by using an Euler-Lagrange approach  
 253 (see He et al. (2017) for details). The FOWT linear model with the TMD is as indicated in (1). Each of the  
 254 three differential equations of the model represents the dynamics of one of the rigid solids sub-systems,  
 255 namely: TMD ( $T$  subindex), tower ( $t$  subindex), and barge platform ( $p$  subindex)

$$\begin{cases}
 I_t \ddot{\theta}_t = m_t g R_t \theta_t - k_t (\theta_t - \theta_p) - d_t (\dot{\theta}_t - \dot{\theta}_p) \\
 \quad - m_T g (R_T \theta_t - x_T) - k_T R_T (R_T \theta_t - x_T) \\
 \quad - d_T R_T (R_T \dot{\theta}_t - \dot{x}_T) \\
 I_p \ddot{\theta}_p = -d_p \dot{\theta}_p - k_p \theta_p - m_p g R_p \theta_p \\
 \quad + k_t (\theta_t - \theta_p) + d_t (\dot{\theta}_t - \dot{\theta}_p) \\
 m_T \ddot{x}_T = k_T (R_T \theta_t - x_T) + m_T g \theta_t \\
 \quad + d_T (R_T \dot{\theta}_t - \dot{x}_T)
 \end{cases} \quad (1)$$

257 This model has three degrees of freedom (DOF): platform pitch angle ( $\theta_p$ ), tower bending angle ( $\theta_t$ )  
 258 and TMD deviation distance,  $x_T$ , the latter regarding the barge and tower absolute rest position, that is also  
 259 known as the (fore-aft) tower top displacement. The  $R_i$  terms represent the distances from the center of

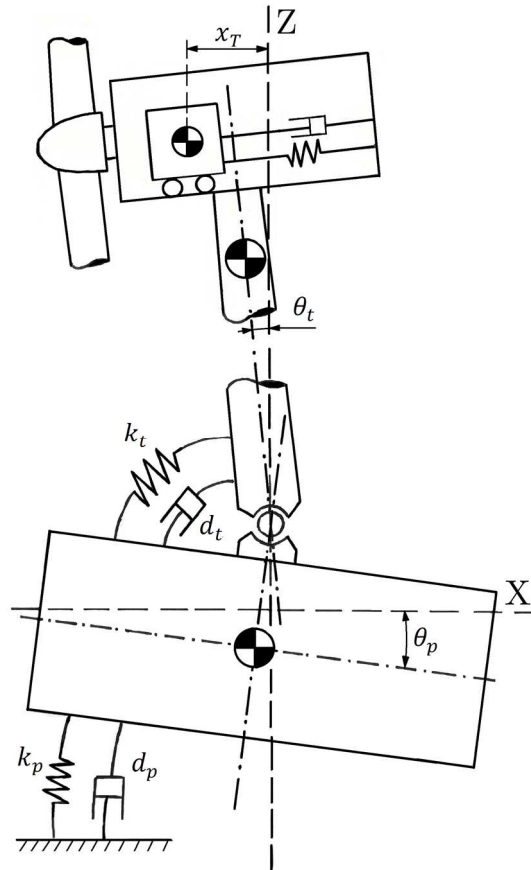
260 mass of each element to the tower-platform virtual hinge point. The tower's flexibility and platform's  
 261 hydrodynamic properties are modeled by a pair of springs,  $k_t$ ,  $k_p$  (N/m), and dampers,  $d_t$ ,  $d_p$  (N·s/m). A  
 262 complete diagram of the system's model is shown in Figure 2.

263 This dynamic model must be characterized for each specific wind turbine through an identification  
 264 process in order to obtain the values of the different coefficients. Due to the lack of available real data, the  
 265 identification of the model parameters was carried out using synthetic data generated by the simulation of  
 266 the floating wind turbine with the aeroelastic computer-aided engineering tool FAST-SC. This software  
 267 allows to generate the wide range of data sets necessary for the identification and validation of the model.  
 268 These data sets were obtained under different conditions to obtain solutions with different configurations.  
 269 The least squares Levenberg-Marquardt algorithm was used for this identification process, taking as input  
 270 FAST free decay tests of 100 secs duration, having the platform an initial pitch angle of 3°. After evaluating  
 271 the identification and validation results in three phases (algorithm, test duration, and initial platform pitch  
 272 selection), the best estimate of the model parameters is obtained. A more detailed description of this  
 273 methodology can be found in Villoslada et al., 2021. The identified parameters were the spring stiffness  $k$   
 274 (N/m), damping coefficient  $d$  (N·s/m), and the inertia moment  $I$  (kg·m<sup>2</sup>), for both the platform ( $p$  subindex)  
 275 and turbine ( $t$  subindex), that is,  $k_p$ ,  $k_t$ ,  $d_p$ ,  $d_t$ ,  $I_p$ , and  $I_t$ . Their identified values are listed in Table 3.

276 Table 3. Identified parameters of the reduced FOWT dynamics model.

$k_t$ (N/m)	$k_p$ (N/m)	$d_t$ (Ns/m)	$d_p$ (Ns/m)	$I_t$ (kg·m <sup>2</sup> )	$I_p$ (kg·m <sup>2</sup> )
$1.4635 \cdot 10^{10}$	$2.0016 \cdot 10^9$	$2.5415 \cdot 10^7$	$5.6431 \cdot 10^7$	$3.4523 \cdot 10^9$	$2.1613 \cdot 10^9$

277 This model was validated with the corresponding one in FAST, and implemented in Matlab so the  
 278 optimal parameters of the passive control devices can be found.



279

280

Figure 2. FOWT model diagram

### 281 3.1 Addition of stops to the FOWT TMD model

282 TMD stops limit the resonant mass stroke. These are used to take into account the available space of  
 283 the stroke of a TMD, thus to make the TMD installation feasible and realistic. These stops are usually  
 284 implemented as a combination of additional spring and damper that start to act when the mass deviates a  
 285 certain distance with respect to its rest position. A diagram of a TMD with stops is shown in Figure 3.

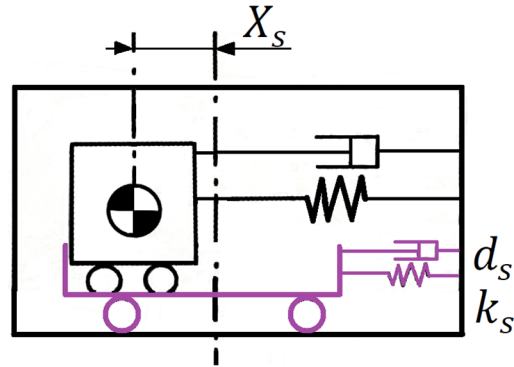


Figure 3. TMD with stops

286  
287

288 The TMD stops can be characterized by three parameters, which in this case have been selected to  
289 ensure compatibility with the ones used in FAST-SC. Although FAST-SC allows to configure every stop  
290 independently, in our scenario the same configuration is applied for both stops, the upwind and the  
291 downwind stops (as if there were a single pair of spring-damper acting at both ends, see Figure 3). The  
292 stops parameters are:

- 293 •  $X_s$  (m): stops actuation distance, measured from the rest position. In FAST-SC, it corresponds to  
294 variables TmdXDWSP and TmdXUWSP, upwind and downwind respectively.
- 295 •  $k_s$  (N/m): stop spring stiffness. In FAST-SC it corresponds to variable TmdXSSpr.
- 296 •  $d_s$  (N·s/m): stop damping coefficient. In FAST-SC it corresponds to variable TmdXSDamp.

297 In addition to the definition of the forces exerted by the stops, attention must be paid to its operational  
298 logic. The same performance implemented in FAST-SC, which was empirically deduced, has been  
299 simulated. In conclusion, the stops can only apply restoring forces on the mass. The spring always acts and  
300 the damper only works when the mass is moving away from its rest position.

301 Considering each stop device independently, the new terms to be added to the model dynamics were  
302 obtained. In the case of the stop spring, a restoring potential force is obtained whenever the mass position  
303 exceeds the actuation distance ( $X_s$ ). Therefore, the spring modifies the system potential energy  $\Delta T$   
304 according to the following expression:

$$305 \quad \Delta T = \begin{cases} +\frac{1}{2}k_s[(R_T \sin \theta_t - x_T) + X_s]^2 & \text{if } (R_T \sin \theta_t - x_T) < -X_s \\ +\frac{1}{2}k_s[(R_T \sin \theta_t - x_T) - X_s]^2 & \text{if } (R_T \sin \theta_t - x_T) > X_s \end{cases} \quad (2)$$

306 This potential energy variation affects the system generalized coordinates,  $\theta_t$  and  $x_T$ , as follows:

$$307 \quad \frac{\partial \Delta T}{\partial \theta_t} = \begin{cases} -k_s R_T \cos \theta_t (R_T \sin \theta_t - x_T + X_s) & \text{if } (R_T \sin \theta_t - x_T) < -X_s \\ -k_s R_T \cos \theta_t (R_T \sin \theta_t - x_T - X_s) & \text{if } (R_T \sin \theta_t - x_T) > X_s \end{cases} \quad (3)$$

$$308 \quad \frac{\partial \Delta T}{\partial x_T} = \begin{cases} -k_s (x_T - R_T \sin \theta_t - X_s) & \text{if } (R_T \sin \theta_t - x_T) < -X_s \\ -k_s (x_T - R_T \sin \theta_t + X_s) & \text{if } (R_T \sin \theta_t - x_T) > X_s \end{cases} \quad (4)$$

309 These expressions can be simplified for small angles as:

$$310 \quad \frac{\partial \Delta T}{\partial \theta_t} = \begin{cases} -k_s R_T (R_T \theta_t - x_T + X_s) & \text{if } (R_T \sin \theta_t - x_T) < -X_s \\ -k_s R_T (R_T \theta_t - x_T - X_s) & \text{if } (R_T \sin \theta_t - x_T) > X_s \end{cases} \quad (5)$$

$$311 \quad \frac{\partial \Delta T}{\partial x_T} = \begin{cases} -k_s (x_T - R_T \theta_t - X_s) & \text{if } (R_T \sin \theta_t - x_T) < -X_s \\ -k_s (x_T - R_T \theta_t + X_s) & \text{if } (R_T \sin \theta_t - x_T) > X_s \end{cases} \quad (6)$$

312 In the case of the stop damper, a non-conservative force acts on the mass. This force is only restoring,  
313 so it is only applicable when the mass is moving away from the rest position. This changes the non-potential  
314 forces in the following way:

$$315 \quad \begin{cases} \Delta Q_{\theta_t} = -d_s R_T (R_T \dot{\theta}_t \cos \theta_t - \dot{x}_T) \\ \Delta Q_{\theta_p} = 0 \\ \Delta Q_{x_T} = d_s (R_T \dot{\theta}_t \cos \theta_t - \dot{x}_T) \end{cases} \quad (7)$$

316 Comparing equations (1) and (7), the damper can be implemented in the model by adding the stop  
317 damping coefficient ( $d_s$ ) to the one of the TMD ( $d_T$ ). The stop damper will act whenever one of the  
318 following position and velocity conditions are satisfied:

$$319 \quad \begin{cases} (R_T \sin \theta_t - x_T) < -X_s \vee (R_T \dot{\theta}_t \cos \theta_t - \dot{x}_T) < 0 \\ (R_T \sin \theta_t - x_T) > X_s \vee (R_T \dot{\theta}_t \cos \theta_t - \dot{x}_T) > 0 \end{cases} \quad (8)$$

#### 320 **4 Optimization case 1: TMD without stops**

321 The FOWT model described in (1) is included in an optimization loop to tune the TMD parameters. The  
322 standard deviation of the Tower Top Displacement in the fore-aft direction,  $\sigma(\text{TTD})$  or  $\sigma(\text{TTD}_{\text{FA}})$ , was used  
323 as fitness function of the genetic algorithm optimization solver. According to other works in the field, the  
324 standard deviation of the tower top fore-aft deflection,  $\sigma(\text{TTD})$  is the most used variable in the TMD  
325 optimization, since variability in  $\text{TTD}_{\text{FA}}$  correlates strongly with fatigue loads in the tower (Lackner and  
326 Rotea, 2011b).

327 Genetic algorithms have been used to find the optimal TMD device parameters as they have been proved  
328 efficient in many similar applications (Alonso-Zotes and Santos Peñas, 2010). All the optimization  
329 processes were implemented in Matlab. The configuration of the GA here applied has a population size of  
330 50 individuals, rank scaling, stochastic uniform selection with a crossover probability of 0.8, and a mutation  
331 probability of 0.01.

332 Each optimization case was set up within an interval for the values of the parameters to be optimized in  
333 order to narrow the search space, so that to ensure convergence and to accelerate the optimization. In  
334 addition, a different resolution for each variable was specified to improve the sensitivity of the optimization  
335 for those variables impacting most the performance. The variation in resolutions allowed to limit the search  
336 space and thus achieving faster convergence of the genetic algorithms. For example, spring stop stiffness  
337 may have lower resolution than TMD spring stiffness. A wide variety of resolution and search space settings  
338 were tested and adapted for each specific scenario, carrying out various optimization rounds with a low  
339 resolution, using a wider search space, and then with higher resolution, in a narrower search space.

340 To explore the advantages and disadvantages of including stops in the TMD, an optimization was run  
341 in the first place without considering the stops, as baseline (referred to as case 1). That sets an optimization  
342 problem with only two variables:  $k_T$  [N/m] and  $d_T$  [N·s/m].

343 Moreover, initially the TMD mass was considered as an optimization variable, but it was found that the  
344 optimal solution always tends to the maximum value (Lackner and Rotea, 2011b). Thus, it was fixed to

345 different values. Table 4 shows the TMD best parameters for different mass values, including information  
 346 about the performance in terms of suppression rate (%), and the resulting stroke (m). The suppression rate  
 347 is the ratio of  $\sigma$ (TTD) reduction with respect to the system response without any structural control with the  
 348 same simulation conditions (100 s, 5° free decay platform pitch). Higher suppression rate means higher  
 349 vibrations absorption. The two bolded values of the mass will be used for the next experiments for  
 350 comparison purposes.

351 Table 4. Optimization results of the TMD without stops

$m_T$ (kg)	$k_T$ (N/m)	$d_T$ (N·s/m)	Suppression Rate (%)	Stroke (m)
5,000	1,246	268	25.5	49.32
10,000	2,424	881	30.06	33.63
<b>20,000</b>	<b>4,568</b>	<b>2,636</b>	<b>34.73</b>	<b>23.57</b>
30,000	6,568	5,436	37.65	18.54
<b>40,000</b>	<b>8,292</b>	<b>9,766</b>	<b>40.06</b>	<b>14.27</b>
50,000	9,693	14,983	42.27	11.39
60,000	11,123	21,812	44.32	9.07

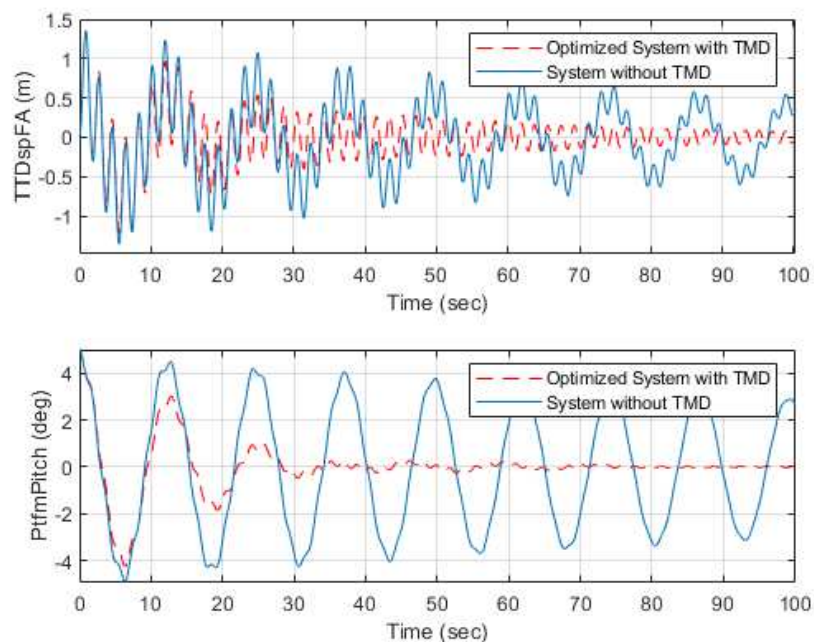
352 The limits and resolution used for the optimization case 1 are shown in Table 5.

353 Table 5. Limits and resolution for optimization case 1

Variable	Resolution	Low limit	High limit
$k_T$ (N/m)	1	0	$10^5$
$d_T$ (N·s/m)	1	0	$10^5$

354 The FOWT response with the optimized  $m_T = 40,000$  kg in comparison to the system without TMD is  
 355 shown in Figure 4. The platform pitch (Figure 4, bottom) is completely stabilized in 35 s with the passive

356 control, whereas without TMD the platform continues oscillating for 800 s. Regarding the Tower Top  
 357 Displacement (TTDspFA) (Figure 4, top), which is composed of two vibration modes, it is possible to see  
 358 that the first dominating mode (related to the platform pitch mode) is damped out substantially more than  
 359 the second mode (related to the tower bending mode). This will be later discussed using the spectral analysis  
 360 of the TTD variable.

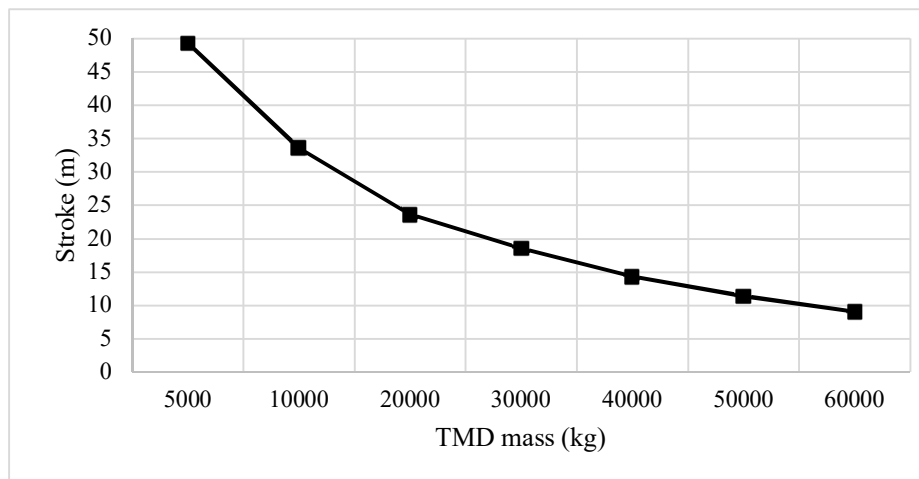


361

362 Figure 4. Simulation of the FOWT with optimized 40 ton TMD (red) and without TMD (blue). Tower  
 363 Top Displacement TTDspFA (top) and Platform Pitch PtfmPitch (bottom).

364 Some authors adjust the spring stiffness coefficient so that the natural undamped frequency of the TMD  
 365 is equal to the first collective platform pitch-tower bending mode (Yang et al., 2019b). This first mode is  
 366 the platform pitch mode and has a frequency of about  $\omega_n=0.086$  Hz, so the corresponding spring stiffness  
 367 for a 40,000 kg TMD would be 11,680 N/m. Although this is a good practice, it seems more convenient to  
 368 include the stiffness as another variable in the optimization loop to find the best value that guarantees a  
 369 global optimum solution to minimize the  $\sigma(\text{TTD})$ . Therefore, the TMD will be optimally tuned not only to  
 370 reduce the first collective platform pitch-tower bending mode, but also the second mode.

371 As already stated, the TMD performance is directly related to its mass. There is an inverse correlation  
 372 between the mass and the resulting stroke. In Figure 5, the stroke length decreases logarithmically with the  
 373 increase of the TMD mass. However, considering that the nacelle is 18 m long, the stops are necessary.  
 374 Note that the stroke length is calculated from the rest position to the maximum separation, so the physical  
 375 space required for a real implementation of the control device would be at least twice the mentioned stroke.  
 376



377

378 Figure 5. Relation between TMD stroke and mass

### 379 5 Optimization of TMD with stops

380 In order to install the TMD in the nacelle, the dimensions of this structural control system including the  
 381 stops must be considered as a constraint in the TMD optimization. This introduces non-linear dynamics to  
 382 the model and three new optimization variables: the distance respect to rest position from which the stops  
 383 start to act,  $X_s$  (m), and its spring and damper coefficients,  $k_s$  (N/m) and  $d_s$  (N·s/m) (Figure 3). The TMD  
 384 non-linearities arise because the stops only act if the mass is displaced from its rest position more than  $X_s$ .  
 385 Moreover, the stop damper only works when the mass is moving away from its rest position.

386 As in the previous case, the FOWT model was included in the optimization loop, with the fatigue given  
 387 by the standard deviation of the TTD, i.e., using  $\sigma(\text{TTD})$  as the fitness function. The system was evaluated  
 388 for free decay tests, with initial platform pitch of  $5^\circ$ . Simulation time is 100 s. In order to address the space

389 limitation constraints, a stroke penalty was added to the fitness function  $F$  (9) to limit those solutions  
 390 exceeding the defined maximum stroke,  $stroke_{max}$ . That is, the stroke penalty is defined to limit the  
 391 maximum stroke of the TMD while allowing the genetic algorithm to optimize the stops position. This  
 392 penalty factor is introduced after confirming that the required unrestricted stroke for a specific case is higher  
 393 than the installation space available. Therefore, the stroke penalty allows to discard unfeasible solutions.

$$394 \quad F = \sigma(TTD) \cdot \left( \frac{10 \cdot stroke}{stroke_{max}} \right) \text{ if } stroke > stroke_{max} \quad (9)$$

395 The configuration of the GA is the same as in the previous experiment, that is, population size of 50  
 396 individuals, rank scaling, stochastic uniform selection with crossover probability of 0.8, and mutation  
 397 probability of 0.01.

398 The TMD mass,  $m_T$ , is not used as an optimization variable as explained before. Two different mass  
 399 values were selected for the experiments, according to the mass ratios used in other works: 20,000 kg and  
 400 40,000 kg. These masses represent 2.8 % and 5.7 % of the wind turbine mass and 0.33 % and 0.65 % of the  
 401 total mass including the barge platform.

402 Two different scenarios were considered, combining the TMD optimization process and the stops:

- 403 • Case 2: Optimization of the TMD parameters considering fixed stops. Variables:  $k_T$  and  $d_T$ .
- 404 • Case 3: Optimization of the TMD parameters and the stops configuration. Variables:  $k_T$ ,  $d_T$ ,  $X_s$ ,  
 405  $k_s$  and  $d_s$ .

### 406 **5.1 Optimization case 2: TMD with fixed stops**

407 In this case 2, stops are not considered in the optimization loop. That is, the stops are fixed and only the  
 408 TMD parameters are optimized. The values of the stops are as proposed in Lackner and Rotea (2011b),  
 409 which have been used in this work as a reference to validate and compare the results. The stop actuation  
 410 distance ( $X_s$ ) was set to 8 m and the spring stiffness ( $k_s$ ) and damper coefficient ( $d_s$ ) were set to  $5 \cdot 10^5$  N/m  
 411 and  $5 \cdot 10^5$  N·s/m, respectively.

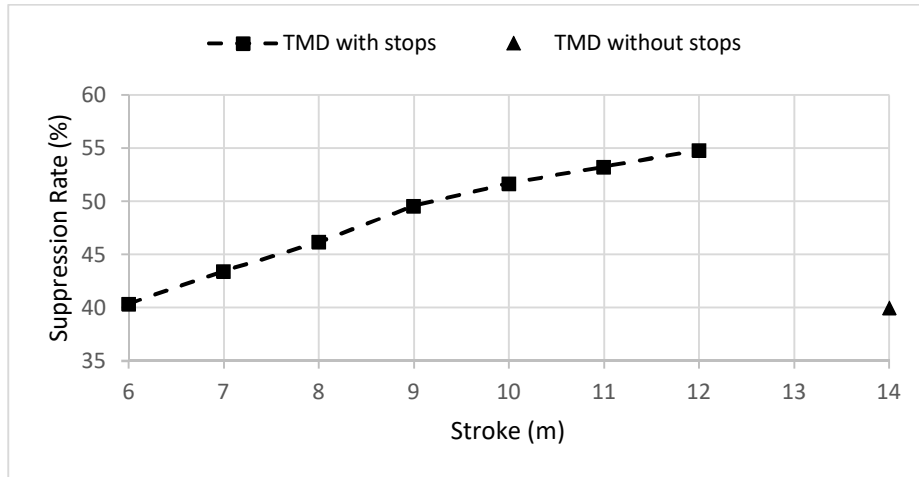
412 Table 6 shows the optimum values and the performance measurements for the two different masses  
 413 selected, and the reference solutions proposed by other authors. To avoid biases due to the use of a different  
 414 model from the one used in the reference studies, and in order to make a fair comparison, the suppression  
 415 rate and stroke were obtained using FAST-SC software (same model for all, free decay test with 5° of  
 416 platform pitch, and simulation time of 100 s).

417 Table 6. Optimization case 2. Solutions and performance

	$m_T$ (kg)	$k_T$ (N/m)	$d_T$ (Ns/m)	<i>Suppression Rate</i> (%)	<i>Stroke</i> (m)
Lackner and Rotea (2011b)	20,000	5,000	9,000	27.49	8.096
Own	20,000	1,423	5,685	30.38	8.191
Stewart and Lackner (2013)	40,000	5,274	10,183	40.43	8.285
Own	40,000	3,943	10,939	44.15	8.373

418  
 419 With both masses, the solutions obtained with our proposal outperform those obtained by other authors.  
 420 This may be due to the precision of the identification model and the design of the optimization process  
 421 (using genetic algorithms and optimizing both  $k_T$  and  $d_T$ ). It is worth noting that the suppression rate in  
 422 the 20,000 kg case did not reach the performance of the TMD without stops (34.73 %). However, with  
 423 40,000 kg, the TMD with stops did surpass the unrestricted TMD solution by 4 %. These optimizations use  
 424 the same resolution and limits as in case 1 (Table 5).

425 It is also interesting to analyze how the stroke affects the TMD performance in comparison with the  
 426 TMD without stops. For this purpose, several optimizations were carried out, obtaining the best possible  
 427 performance for different strokes (varying  $X_s$  and  $\text{stroke}_{\max}$ ). The results for a TMD mass value of 40,000  
 428 kg are shown in Figure 6.



429

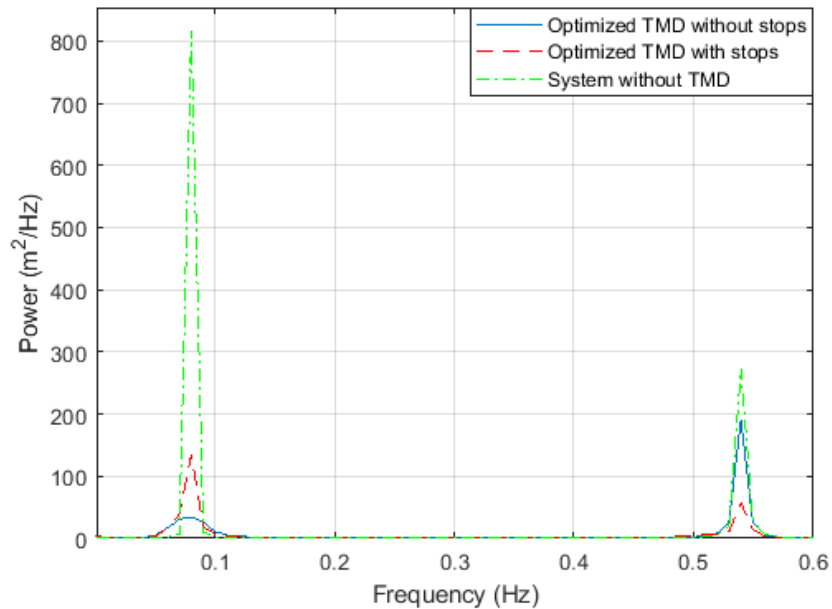
430

Figure 6. Suppression rate as a function of the stroke

431 Surprisingly, with this large TMD, the stops help to limit the TMD displacement along its track and also  
 432 increase the suppression rate. The reason behind the vibration reduction when stops are limiting the TMD  
 433 stroke can be found through an analysis of the response in the frequency domain. Figure 7 shows the power  
 434 spectral density of the TTD variable in three cases:

- 435 i) the baseline system without structural control (green),
- 436 ii) the system with TMD without stops (blue)
- 437 iii) the system with TMD with stops (red).

438 All these control solutions were tested for a TMD mass of 40,000 kg and an initial pitch angle of 5° for  
 439 a time interval of 100 seconds.



440

441

Figure 7. PSD of the TTD variable for the baseline system and the TMD solutions

442

443

444

445

446

447

The tower top displacement presents two modes, which correspond to the first and second collective platform pitch-tower bending modes, respectively. Both TMD solutions, with and without stops, are beneficial in reducing the system vibrations, but they achieve this objective in different ways. On one hand, the TMD without stops reduces significantly the first mode, which is the predominant one, to a magnitude lower than the second mode. On the other hand, the TMD with stops mitigates the first mode but it also reduces the second mode.

448

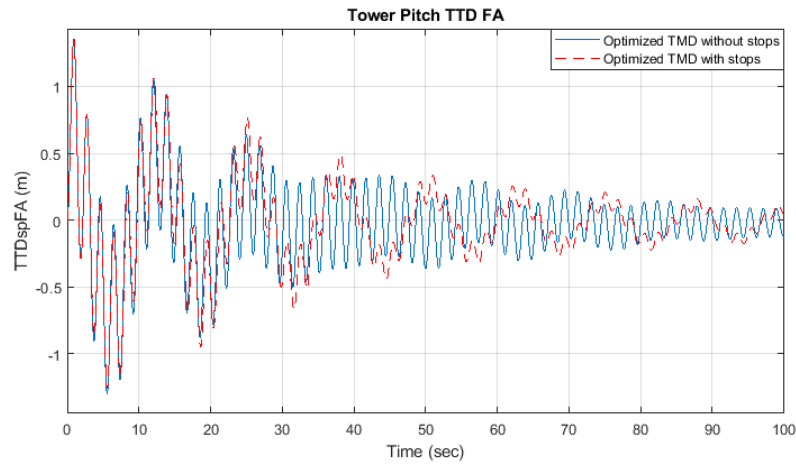
449

450

451

The response of the FOWT with both TMD solutions in the time domain is shown in Figure 8. The differences in performance (with and without stops) are evident; the TMD with stops reduces the second oscillation mode (high frequency) while the TMD without stops acts predominantly on the first mode (low frequency component).

452



453

454

Figure 8. TTD of the floating wind turbine with TMD, with and without stops

455

456

457

458

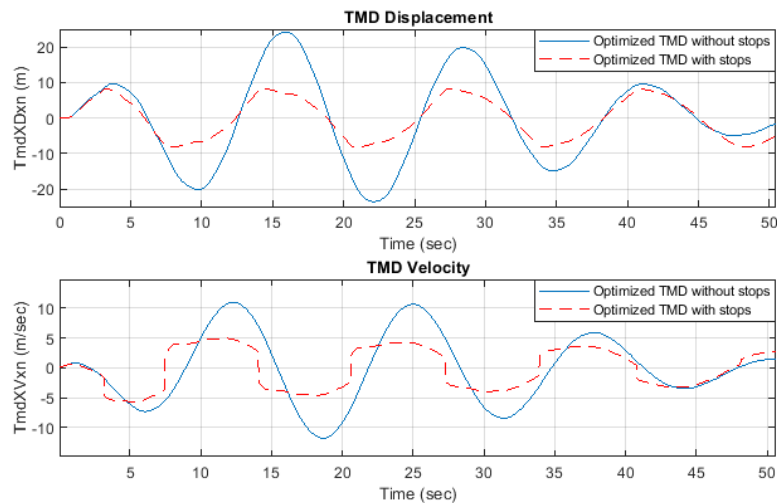
459

460

461

462

According to the model of the system, the dynamics of the TMD with stops are different from the case of the TMD without them. This can be anticipated by observing the variation in the stiffness and damping parameters. With stops, the TMD spring stiffness is considerably lower since it is no longer the only responsible for stopping the oscillating mass. The damping coefficient is larger with stops, specifically in the case of 20,000 kg of TMD mass. Figure 9 shows the displacements (m) (top) and speeds (m/s) (bottom) of the TMD optimum solution, with and without stops, for a mass of 20,000 kg. These data were obtained by simulating a free decay test of 5 ° platform pitch with FAST-SC for 100 seconds.



463  
 464 Figure 9. TMD displacement (top) and velocity (bottom), with (dashed red line) and without (blue  
 465 line) stops

466 In addition to the reduction of TMD displacement, the change in the TMD velocity is noticeable (Figure  
 467 9, bottom). From a sinusoidal shape in the case of TMD without stops, it becomes a square waveform -of  
 468 the same frequency- when stops are added. This may be because the stops induce an abrupt change of  
 469 direction on the mass. The optimal solution with stops reaches a larger absolute average speed along the  
 470 oscillation track, thus allowing the damper to absorb more energy.

### 471 5.3 Optimization case 3: TMD with optimized stops

472 Once the benefits of the addition of stops have been shown, their configuration is included in the  
 473 optimization process to get the maximum vibration reduction. As already said, this adds three new variables  
 474 to the optimization: the stops distance ( $X_s$ ), the stops spring stiffness ( $k_s$ ), and the stops damper coefficient  
 475 ( $d_s$ ).

476 The parameters obtained in this optimization case 3 are shown in Table 7, while the performance  
 477 measures (suppression rate and stroke) of the TMD is shown in Table 8, along with the three other  
 478 optimization cases for comparison purposes.

479

480

Table 7. Optimization case 3. Solutions

$m_T$ (kg)	$k_T$ (N/m)	$d_T$ (Ns/m)	$X_s$ (m)	$k_s$ (N/m)	$d_s$ (Ns/m)
20,000	1,877	6,174	8.09	502,900	893,400
40,000	2,197	11,614	8.00	499,600	315,200

481

482

Table 8. Performances comparison of all TMD configurations

Configuration (case)	$m_T$ (kg)	Suppression Rate (%)	Stroke (m)
TMD w/o stops (1)	20,000	34.24	23.6
TMD w/ fixed stops (2)	20,000	30.38	8.2
TMD w/ optimized stops (3)	20,000	31.88	8.2
TMD w/o stops (1)	40,000	40.00	14.3
TMD w/ fixed stops (2)	40,000	44.15	8.4
TMD w/ optimized stops (3)	40,000	44.79	8.4

483

484

In this third case, several optimizations were run, starting from low resolution -wider search space

485

(Table 9), and then moving on to a higher resolution –narrower search space (Table 10 and Table 11), with

486

different TMD masses.

487

Table 9. Low resolution - wide search limits configuration

Variable	Resolution	Low limit	High limit
$k_T$ (N/m)	10	100	$10^5$

$d_T$ (Ns/m)	10	100	$10^5$
$X_S$ (m)	0.1	9.0	5.0
$k_S$ (N/m)	100	100	$10^6$
$d_S$ (s/m)	100	100	$10^6$

488

489

Table 10. High resolution - narrow search limits configuration (20,000 kg)

Variable	Resolution	Low limit	High limit
$k_T$ (N/m)	1	$10^3$	$5 \cdot 10^3$
$d_T$ (Ns/m)	1	$3 \cdot 10^3$	$10^4$
$X_S$ (m)	0.01	7.80	8.30
$k_S$ (N/m)	100	$10^4$	$10^6$
$d_S$ (s/m)	100	$10^4$	$10^6$

490

491

Table 11. High resolution - narrow search limits configuration (40,000 kg)

Variable	Resolution	Low limit	High limit
$k_T$ (N/m)	1	$10^3$	$10^4$
$d_T$ (Ns/m)	1	$10^3$	$2 \cdot 10^4$
$X_S$ (m)	0.01	7.50	8.50
$k_S$ (N/m)	100	$10^3$	$10^6$

$d_s$  (s/m)            100             $10^3$              $10^6$

492

493        With the two different TMD masses considered, better solutions are obtained when optimizing the stops  
 494 configuration. The improvement in terms of suppression rate, with respect to the fixed stop configuration  
 495 (case 2) is 1.5 % and 0.64 % for TMD masses of 20,000 kg and 40,000 kg, respectively. Consequently, it  
 496 is possible to conclude that the improvement provided by the stops' optimization increases with the stroke  
 497 limitation with respect to the ideal TMD stroke without stops. This means that smaller/lighter TMDs, which  
 498 require a longer stroke, will benefit more from the optimization of the stops' configuration.

#### 499    **6 Conclusions and future works**

500        This paper addresses a real requirement of passive control. It is a step forward towards the design and  
 501 implementation of devices that could reduce the impact of vibrations in floating wind turbines and that may  
 502 attract industrial and commercial interest. In addition to this, exploring the use of these control devices will  
 503 help reduce maintenance costs and increase the efficiency of floating wind turbines. The investigation on  
 504 this solution not only fosters the use of renewable energies but proposing feasible solutions makes it more  
 505 attractive and competitive for the wind industry.

506        The main contribution of this paper is to consider the stops that limit the stroke on a TMD control device  
 507 to be included in an optimization loop. It has been proved that with this methodology good vibration  
 508 suppression rates are achieved in comparison to cases that consider fixed stops or even without stops.

509        The optimization process of the stops, together with the TMD tuning parameters is advisable for any  
 510 application that has to deal with strokes and mass constrains. These findings are not restricted to FOWT,  
 511 but they can be applied to any other system to enhance the performance of passive structural TMD control.

512        Further studies could be focused on advanced structural control techniques, such as semi-active or active  
 513 ones. Additionally, performing simulations under different wind and wave load conditions, as well as  
 514 testing the proposals on real prototypes would be desirable. Finally, the use of more than one TMD acting  
 515 cooperatively or being installed in different parts of the structure could be addressed.

516 **Funding**

517 This work was partially supported by the Spanish Ministry of Science, Innovation and Universities under  
518 MCI/AEI/FEDER Project number RTI2018-094902-B-C21.

519 **Author contributions**

520 **Villoslada, D.:** Conceptualization; Investigation; Software; Validation; Visualization; Writing - original  
521 draft. **Santos, M.:** Conceptualization; Investigation; Methodology; Funding acquisition; Writing - review  
522 & editing. **Tomás-Rodríguez, M.:** Conceptualization; Investigation; Methodology; Writing - review &  
523 editing.

524 **References**

- 525 Alonso-Zotes, F., Santos, M., 2017. Heuristic optimization of interplanetary trajectories in aerospace  
526 missions. *Revista Iberoamericana de Automática e Informática Industrial* 14(1), 1-15.
- 527 Caglayan, D. G., Ryberg, D. S., Heinrichs, H., Linßen, J., Stolten, D., & Robinius, M., 2019. The techno-  
528 economic potential of offshore wind energy with optimized future turbine designs in Europe. *Applied*  
529 *Energy*, 255, 113794.
- 530 Chen, X., Kareem, A., Xu, G., Wang, H., Sun, Y., & Hu, L., 2021. Optimal tuned mass dampers for wind  
531 turbines using a Sigmoid satisfaction function-based multiobjective optimization during earthquakes.  
532 *Wind Energy*.
- 533 Cong, C., 2019. Using active tuned mass dampers with constrained stroke to simultaneously control  
534 vibrations in wind turbine blades and tower. *Advances in Structural Engineering*, 22(7), 1544-1553.
- 535 Costoya, X., DeCastro, M., Carvalho, D., & Gómez-Gesteira, M., 2020. On the suitability of offshore wind  
536 energy resource in the United States of America for the 21st century. *Applied Energy*, 262, 114537.
- 537 Dinh, V. N., & Basu, B. 2015. Passive control of floating offshore wind turbine nacelle and spar vibrations  
538 by multiple tuned mass dampers. *Structural Control and Health Monitoring*, 22(1), 152-176.

- 539 Galán-Lavado, A., & Santos, M., 2021. Analysis of the effects of the location of passive control devices on  
540 the platform of a floating wind turbine. *Energies*, 14(10), 2850.
- 541 He, E. M., Hu, Y. Q., Zhang, Y., 2017. Optimization design of tuned mass damper for vibration suppression  
542 of a barge-type offshore floating wind turbine. *Proc. of the Institution of Mechanical Engineers, Part*  
543 *M: Journal of Engineering for the Maritime Environment*, 231(1), 302-315.
- 544 Hu, Y., & He, E., 2017. Active structural control of a floating wind turbine with a stroke-limited hybrid  
545 mass damper. *Journal of Sound and Vibration*, 410, 447-472.
- 546 Jonkman, J. M., & Buhl Jr, M. L., 2007. Loads analysis of a floating offshore wind turbine using fully  
547 coupled simulation (No. NREL/CP-500-41714). National Renewable Energy Lab.(NREL), Golden,  
548 CO (United States).
- 549 Jonkman, J. M., 2007. Dynamics modeling and loads analysis of an offshore floating wind turbine (No.  
550 NREL/TP-500-41958). National Renewable Energy Lab.(NREL), Golden, CO (United States).
- 551 Jonkman, J., Butterfield, S., Musial, W., Scott, G., 2009. Definition of a 5-MW reference wind turbine for  
552 offshore system development (No. NREL/TP-500-38060). National Renewable Energy Lab.(NREL),  
553 Golden, CO (United States).
- 554 Lackner, M. A., & Rotea, M. A., 2011a. Structural control of floating wind turbines. *Mechatronics*, 21(4),  
555 704-719.
- 556 Lackner, M. A., & Rotea, M. A., 2011b. Passive structural control of offshore wind turbines. *Wind*  
557 *energy*, 14(3), 373-388.
- 558 Li, C., Zhuang, T., Zhou, S., Xiao, Y., & Hu, G., 2017. Passive vibration control of a semi-submersible  
559 floating offshore wind turbine. *Applied Sciences*, 7(6), 509.
- 560 Liao, M., & Wu, Y., 2020. Conceptual design and dynamic analysis of a novel passive floating offshore  
561 wind turbine structure. *Ships and Offshore Structures*, 1-10.

- 562 Mikati, M., Santos, M., & Armenta, C., 2013. Electric grid dependence on the configuration of a small-  
563 scale wind and solar power hybrid system. *Renewable energy*, 57, 587-593.
- 564 Olondriz, J., Jugo, J., Elorza, I., & Aron Pujana-Arrese, S. A. Q., 2019. A feedback control loop  
565 optimisation methodology for floating offshore wind turbines. *Energies*, 12(18), 3490.
- 566 Park, S., Lackner, M. A., Pourazarm, P., Rodríguez Tsouroukdissian, A., & Cross-Whiter, J., 2019. An  
567 investigation on the impacts of passive and semiactive structural control on a fixed bottom and a  
568 floating offshore wind turbine. *Wind Energy*, 22(11), 1451-1471.
- 569 Pimenta, F., Ruzzo, C., Failla, G., Arena, F., Alves, M., & Magalhães, F., 2020. Dynamic Response  
570 Characterization of Floating Structures Based on Numerical Simulations. *Energies*, 13(21), 5670.
- 571 Rubio, P. M., Quijano, J. F., López, P. Z., 2019. Intelligent control for improving the efficiency of a hybrid  
572 semi- submersible platform with wind turbine and wave energy converters. *Revista Iberoamericana  
573 de Automática e Informática Industrial* 16(4), 480–491.
- 574 Saaed, T. E., Nikolakopoulos, G., Jonasson, J. E., Hedlund, H., 2015. A state-of-the-art review of structural  
575 control systems. *Journal of Vibration and Control*, 21(5), 919-937.
- 576 Sierra-García, J.E., Santos M., 2020a. Performance analysis of a wind turbine pitch neurocontroller with  
577 unsupervised learning. *Complexity* 2020 (2020).
- 578 Sierra-García, J.E., Santos M., 2020b. Exploring reward strategies for wind turbine pitch control by  
579 reinforcement learning. *Applied Sciences* 10(21), 7462.
- 580 Sierra-García, J.E., Santos M., 2021. Neural networks and reinforcement learning in wind turbine  
581 control. *Revista Iberoamericana de Automática e Informática industrial*, 18(4), 327-335.
- 582 Stewart, G., Lackner, M., 2013. Offshore wind turbine load reduction employing optimal passive tuned  
583 mass damping systems. *IEEE transactions on control systems technology*, 21(4), 1090-1104. DOI:  
584 10.1109/TCST.2013.2260825

- 585 Tomás-Rodríguez, M., & Santos, M., 2019. Modelling and control of floating offshore wind  
586 turbines. *Revista Iberoamericana de Automática e Informática industrial*, 16(4), 381-390.
- 587 Vijfhuizen, W., 2006. Design of a wind and wave power barge. Universities of Glasgow and Strathclyde,  
588 Glasgow, Scotland.
- 589 Villoslada, D., M. Santos, and M. Tomas-Rodriguez., 2020. Inerter-based Passive Structural Control for  
590 Barge Floating Offshore Wind Turbines. *IFAC-PapersOnLine* 53.2: 12358-12363.
- 591 Villoslada, D., Santos, M., & Tomás-Rodríguez, M., 2021. General methodology for the identification of  
592 reduced dynamic models of barge-type floating wind turbines. *Energies*, 14(13), 3902.
- 593 Wang, C. M., Utsunomiya, T., Wee, S. C., & Choo, Y. S., 2010. Research on floating wind turbines: a  
594 literature survey. *The IES Journal Part A: Civil & Structural Engineering*, 3(4), 267-277.
- 595 Xie, S., Jin, X., & He, J., 2019a. Structural vibration control for the offshore floating wind turbine including  
596 drivetrain dynamics analysis. *Journal of Renewable and Sustainable Energy*, 11(2), 023304.
- 597 Xie, S., Jin, X., He, J., & Zhang, C., 2019b. Structural responses suppression for a barge-type floating wind  
598 turbine with a platform-based TMD. *IET Renewable Power Generation*, 13(13), 2473-2479.
- 599 Yang, W., Tian, W., Hvalbye, O., Peng, Z., Wei, K., & Tian, X., 2019a. Experimental research for  
600 stabilizing offshore floating wind turbines. *Energies*, 12(10), 1947.
- 601 Yang, J., He, E. M., & Hu, Y. Q., 2019b. Dynamic modeling and vibration suppression for an offshore  
602 wind turbine with a tuned mass damper in floating platform. *Applied Ocean Research*, 83, 21-29.
- 603 Yang, J. J., & He, E. M., 2020. Coupled modeling and structural vibration control for floating offshore  
604 wind turbine. *Renewable Energy*, 157, 678-694.
- 605 Zuo, H., Bi, K., & Hao, H., 2020. A state-of-the-art review on the vibration mitigation of wind turbines.  
606 *Renewable and Sustainable Energy Reviews*, 121, 109710.